

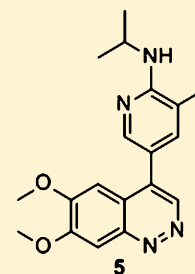
## Rapid Identification of a Novel Small Molecule Phosphodiesterase 10A (PDE10A) Tracer

Essa Hu,<sup>\*,†</sup> Ji Ma,<sup>#</sup> Christopher Biorn,<sup>‡</sup> Dianna Lester-Zeiner,<sup>‡</sup> Robert Cho,<sup>#</sup> Shannon Rumfelt,<sup>†</sup> Roxanne K. Kunz,<sup>†</sup> Thomas Nixey,<sup>†</sup> Klaus Michelsen,<sup>§</sup> Silke Miller,<sup>‡</sup> Jianxia Shi,<sup>#</sup> Jamie Wong,<sup>#</sup> Geraldine Hill Della Puppa,<sup>‡</sup> Jessica Able,<sup>‡</sup> Santosh Talreja,<sup>‡</sup> Dah-Ren Hwang,<sup>||</sup> Stephen A. Hitchcock,<sup>†,∞</sup> Amy Porter,<sup>‡</sup> David Immke,<sup>‡</sup> Jennifer R. Allen,<sup>†</sup> James Treanor,<sup>‡</sup> and Hang Chen<sup>\*,‡</sup>

<sup>†</sup>Department of Small Molecule Chemistry, <sup>‡</sup>Department of Neuroscience, <sup>§</sup>Department of Molecular Structures, and <sup>||</sup>Department of Medical Sciences, Amgen Inc., One Amgen Center Drive, Thousand Oaks, California 91320-1799, United States

<sup>‡</sup>Department of Neuroscience and <sup>#</sup>Department of Pharmacokinetics and Drug Metabolism, Amgen Inc., 1120 Veterans Boulevard, South San Francisco, California 94080, United States

**ABSTRACT:** A radiolabeled tracer for imaging therapeutic targets in the brain is a valuable tool for lead optimization in CNS drug discovery and for dose selection in clinical development. We report the rapid identification of a novel phosphodiesterase 10A (PDE10A) tracer candidate using a LC–MS/MS technology. This structurally distinct PDE10A tracer, AMG-7980 (**5**), has been shown to have good uptake in the striatum (1.2% ID/g tissue), high specificity (striatum/thalamus ratio of 10), and saturable binding in vivo. The PDE10A affinity ( $K_D$ ) and PDE10A target density ( $B_{max}$ ) were determined to be 0.94 nM and 2.3 pmol/mg protein, respectively, using [<sup>3</sup>H]**5** on rat striatum homogenate. Autoradiography on rat brain sections indicated that the tracer signal was consistent with known PDE10A expression pattern. The specific binding of [<sup>3</sup>H]**5** to rat brain was blocked by another structurally distinct, published PDE10A inhibitor, MP-10. Lastly, our tracer was used to measure in vivo PDE10A target occupancy of a PDE10A inhibitor in rats using LC–MS/MS technology.



## INTRODUCTION

Radiotracers have been used in clinical studies as biomarkers to determine target coverage in the human brain. Molecular imaging approaches using target-specific, well-behaved PET (positron emission tomography) or SPECT (single-photon emission computed tomography) radiotracers have generated valuable data, providing researchers with a noninvasive method to correlate CNS target coverage with drug pharmacokinetics (PK) in the plasma, to facilitate clinical design and to help interpret clinical outcomes.<sup>1</sup> Despite their demonstrated utility in the clinic, use of radiotracers in CNS preclinical drug discovery efforts has been limited because of challenges of developing a novel target specific radiotracer. In addition to high intrinsic potency and brain permeability, radiotracers must also exhibit high specificity, high brain uptake, and suitable target binding kinetics. Nevertheless, a target-specific radiotracer can be a very powerful translational tool in preclinical research, allowing the measurement of binding characteristics of the target ( $K_D$  and  $B_{max}$ ) in tissues across species as well as enabling assessment of target occupancy during the lead optimization. Furthermore, such a tool can be used to correlate target occupancy of a drug candidate with preclinical efficacy and target engagement experiments to support dose selection in clinical studies.

The impetus to develop a radiotracer for preclinical research stemmed from our interest in developing an inhibitor for phosphodiesterase 10A (PDE10A) for the treatment of schizophrenia. Phosphodiesterase 10A is a hydrolase that

cleaves the cyclic 3',5'-phosphodiester bonds of cyclic adenosine monophosphate (cAMP) and cyclic guanosine monophosphate (cGMP) to generate adenosine monophosphate (AMP) and guanosine monophosphate (GMP).<sup>2</sup> PDE10A is most highly expressed in the GABAergic medium spiny neurons of the striatum which is the main relay for glutamatergic cortical input and dopaminergic input within the basal ganglia.<sup>3</sup> Phenotypic analyses of PDE10A knockout mice (PDE10A<sup>-/-</sup>)<sup>4</sup> have shown that these mice have dampened responses in models of psychosis and disrupted basal ganglia function. Furthermore, TP-10<sup>4</sup> and MP-10<sup>5</sup> (Figure 1), both selective inhibitors of

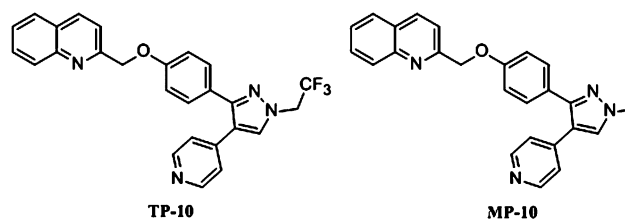
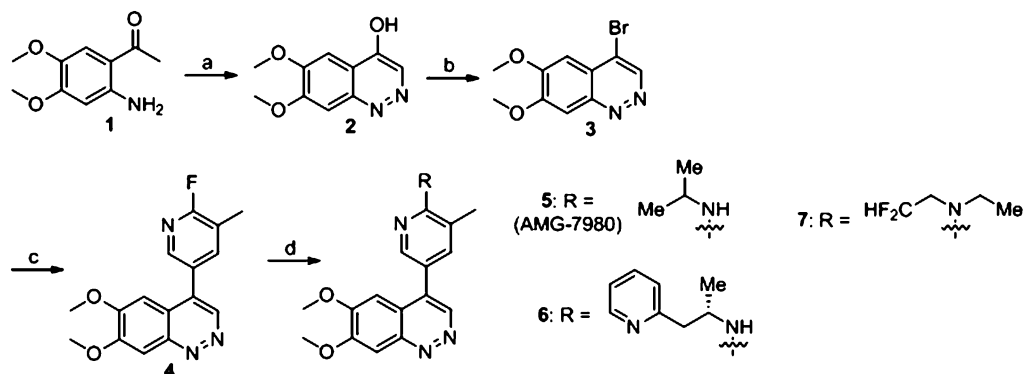


Figure 1.

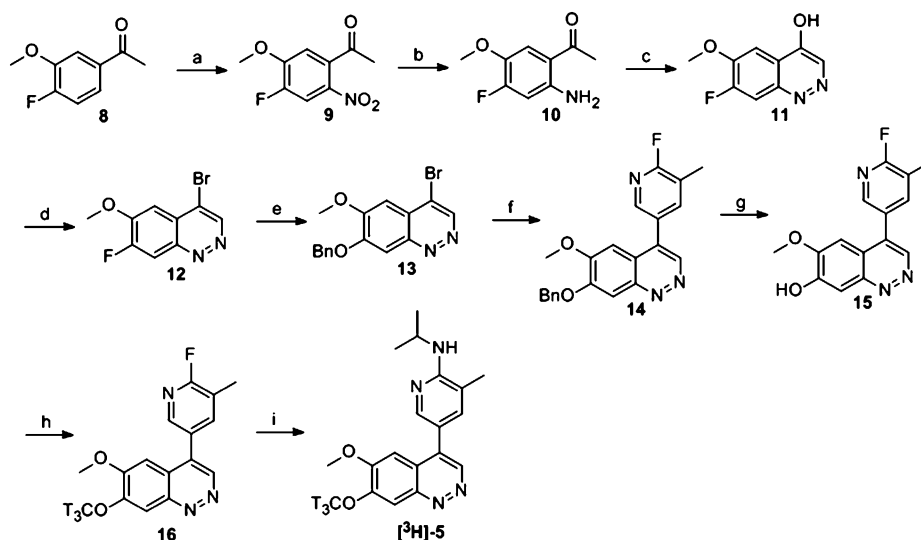
PDE10A, have been reported to be efficacious in preclinical rodent behavioral models of schizophrenia such as phencyclidine (PCP) stimulated hyperlocomotor activity model, prepulse inhibition model (PPI), and conditioned avoidance

Received: February 22, 2012

Published: May 1, 2012

Scheme 1. Synthesis of Tracer Candidates 5, 6, and 7<sup>a</sup>

<sup>a</sup>Reagents and conditions: (a) NaNO<sub>2</sub>, HCl, water, 75 °C, 71% yield; (b) POBr<sub>3</sub>, MeCN, 70 °C, 77% yield; (c) Cs<sub>2</sub>CO<sub>3</sub>, Pd(PPh<sub>3</sub>)<sub>4</sub>, DME, water; 75% yield; (d) for **5**, propan-2-amine, K<sub>2</sub>CO<sub>3</sub>, DMSO, 90 °C, 71% yield; (i) for **6**, 2,2-difluoroethanamine, K<sub>2</sub>CO<sub>3</sub>, DMSO, 90 °C, 45% yield; (ii) NaH, EtI, DMF, 48% yield; for **7**, 1-(pyridin-2-yl)propan-2-amine, K<sub>2</sub>CO<sub>3</sub>, DMSO, 90 °C, then chiral separation by SFC.

Scheme 2. Synthesis of Precursor 15 and Subsequent Radiosynthesis of [<sup>3</sup>H]**5**<sup>a</sup>

<sup>a</sup>Reagents and conditions: (a) acetic anhydride, nitric acid, 82% yield; (b) AcOH, iron, 89% yield; (c) NaNO<sub>2</sub>, HCl, water, 65 °C, 91% yield; (d) POBr<sub>3</sub>, 41% yield; (e) LHMDS, BnOH, 50 °C, 47% yield; (f) Na<sub>2</sub>CO<sub>3</sub>, Pd(PPh<sub>3</sub>)<sub>2</sub>Cl<sub>2</sub>, DME, water; (g) H<sub>2</sub>, Pd/C; (h) K<sub>2</sub>CO<sub>3</sub>, CT<sub>3</sub>I; (i) propan-2-amine, K<sub>2</sub>CO<sub>3</sub>, DMSO, 90 °C.

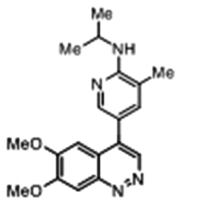
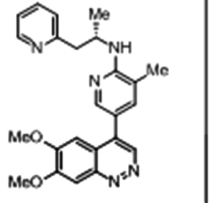
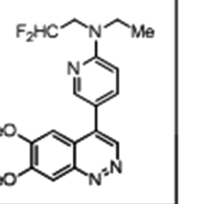
response (CAR).<sup>6</sup> These results support the concept that inhibition of PDE10A could have therapeutic benefit in neurological disorders, including schizophrenia, Parkinson's disease, and Huntington's disease.<sup>7</sup>

Traditionally, a tracer candidate has to be radiolabeled prior to any in vivo kinetics profiling. The need to radiolabel multiple candidates and the need to develop different synthetic routes to enable radiolabeling prior to tracer selection make this approach both time and cost prohibitive. Instead, we directly evaluated the kinetics of unlabeled compounds in vivo by utilizing a method based upon a liquid chromatography coupled to mass spectrometry (LC–MS) technology, first reported by Phebus et al.<sup>8</sup> to evaluate profiles of known tracers in rats. Using both a set of in vitro profile criterion to identify brain penetrant compounds and this LC–MS technology to measure brain distribution, we have rapidly identified **5** (AMG-7980)<sup>9</sup> as the optimal tracer. Further in vivo studies confirmed suitable kinetic properties of the tracer.

## RESULTS AND DISCUSSION

**Chemistry and Radiochemistry.** Syntheses of the three tracer candidates discussed in this report are described in Scheme 1. All three compounds shared the same core scaffold. The commercially available 1-(2-amino-4,5-dimethoxyphenyl)ethanone (**1**) was heated with sodium nitrite to produce 6,7-dimethoxycinnolin-4-ol (**2**) in 71% yield. The resulting phenol was subjected to phosphorus oxybromide to generate 4-bromo-6,7-dimethoxycinnoline (**3**). Suzuki coupling with (6-fluoro-5-methylpyridin-3-yl)boronic acid afforded the 4-(6-fluoro-5-methylpyridin-3-yl)-6,7-dimethoxycinnoline scaffold (**4**). Tracer candidates **5** and **7** were synthesized by S<sub>N</sub>Ar displacement of pyridyl fluoride in DMSO with propan-2-amine and 1-(pyridin-2-yl)propan-2-amine, respectively. Enantiopure tracer **7** was isolated after chiral separation of racemic mixture **5**-(6,7-dimethoxycinnolin-4-yl)-3-methyl-*N*-(1-(pyridin-2-yl)propan-2-yl)pyridin-2-amine using supercritical fluid chromatography (SFC). Candidate **6** was obtained in two steps starting with a similar S<sub>N</sub>Ar displacement of intermediate **4** with 2,2-difluoroethanamine followed by alkylation with iodoethane.

Table 1. Summary of Tracer Candidates Properties

|  |  |  |  |
|--|---|--|---|
| Compound#  | 5   | 6  | 7   |
| cLogP  | 3.1   | 3.9  | 3.8   |
| <i>In vitro</i> potency<br>PDE10 IC <sub>50</sub> (nM)<br>PDE selectivity        | 1.9<br>>700x  | 0.8<br>>2400x  | 5.7<br>>1200x   |
| Permeability<br>LLC-PK1 (μm/s)<br>Rat p-gp efflux ratio                          | 24.7<br>1.1   | 9.9<br>1.0   | 38<br>0.7   |
| LC-MS/MS<br>AUC Ratio (striatum/thalamus)<br>% Injected dose/g tissue (striatum) | 9.4<br>1.2  | 11.8<br>0.3  | 2.6<br>1.1  |

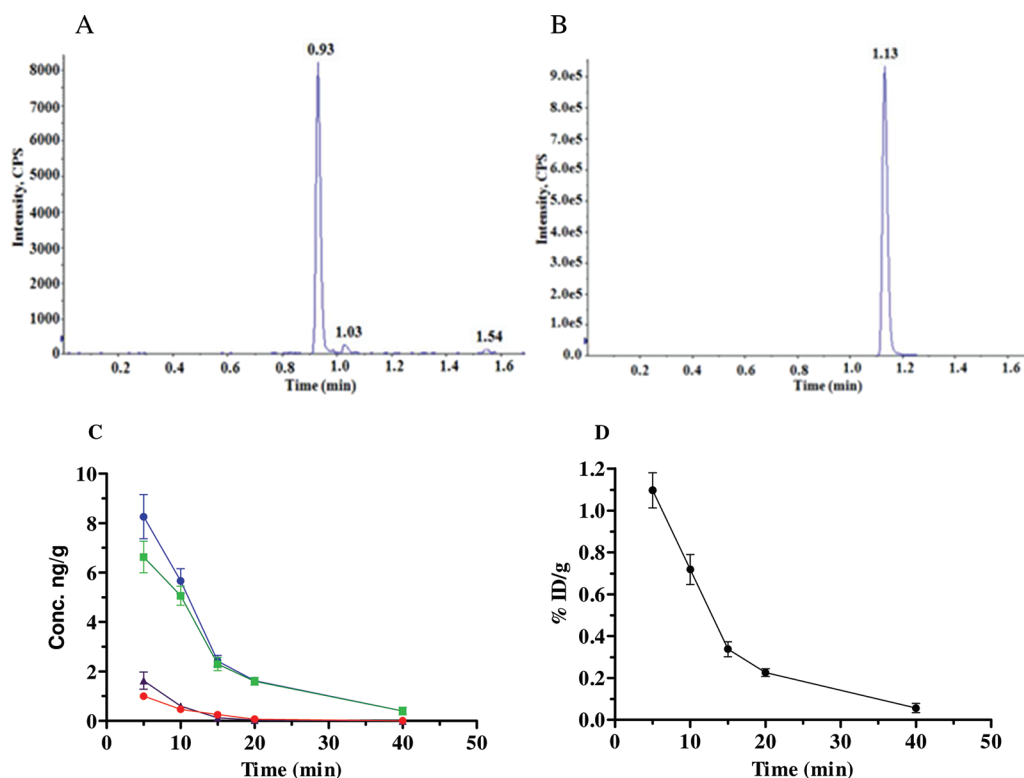


**Figure 2.** LC–MS/MS tracer kinetics distribution of **5** in vivo in rats. (A) Peak intensity in striatal tissue. LC–MS/MS quantification of **5** was done by measuring MRM transition of  $m/z$  391.1–281.0. (B) Peak intensity of internal control. (C) Time course and tissue distribution of **5** in vivo in rats. The concentrations of **5** in striatum (blue circle), thalamus (purple triangle), and plasma (red dot) were measured by LC–MS/MS. Green squares represent specific uptake (striatum minus thalamus). (D) Percentage of injected dose per gram of tissue (% ID/g) in the target tissue (striatum). Error bars represent standard error of mean, and  $N = 4$  animals per group.

Rodent metabolite identification (ID) studies suggested that the 7-methoxy group on the cinnoline was a suitable position for tritium radiolabeling. In the original synthetic route (Scheme 1), this 7-methoxy group was introduced in the first step. To maximize the radiochemical yield of [ $^3\text{H}$ ]**5**, we designed a different synthetic route in order to reduce the number of steps after tritium labeling (Scheme 2). Our redesigned synthetic route began with nitration of commercially

available 1-(4-fluoro-3-methoxyphenyl)ethanone (**8**) to produce 1-(4-fluoro-5-methoxy-2-nitrophenyl)ethanone (**9**). Iron reduction afforded 1-(2-amino-4-fluoro-5-methoxyphenyl)ethanone (**10**). Cyclization with sodium nitrite formed 7-fluoro-6-methoxycinnolin-4-ol (**11**). Reflux with phosphorus oxybromide generated 4-bromo-7-fluoro-6-methoxycinnoline (**12**). Treatment of sodium benzylate with 4-bromo-7-fluoro-6-methoxycinnoline produced the protected 7-(benzyloxy)-4-

bromo-6-methoxycinnoline (13). After Suzuki coupling to make 7-(benzyloxy)-4-(6-fluoro-5-methylpyridin-3-yl)-6-methoxycinnoline (14), radiolabel precursor cinnolin-7-ol (15) was unmasked by palladium hydrogenation. Tritiation with [<sup>3</sup>H]methyl iodide followed by S<sub>N</sub>Ar displacement with propan-2-amine produced the tritiated radiotracer [<sup>3</sup>H]5.

**Pharmacology.** Three tracer candidates 5, 6, and 7, were selected from our collection of PDE10A inhibitors for advancement into in vivo studies. These compounds were chosen based on a set of in vitro and physicochemical criteria:<sup>10</sup> single-digit nanomolar IC<sub>50</sub> potency on PDE10A, greater than 100-fold selectivity over other PDEs, moderate lipophilicity (log *P* of 1–4), and good permeability devoid of P-gp substrate recognition (P-gp efflux ratio of <3) (Table 1). These parameters were selected to ensure that the tracer candidates would be specific to PDE10A and CNS permeable.

**LC–MS/MS Tracer Kinetics.** We employed the LC–MS/MS based technology platform developed by Phebus et al.<sup>7</sup> to evaluate the binding kinetics of these tracer candidates in rats using unlabeled compounds. Unlabeled compound was administered as a microdose (3–10 μg/kg) in rats by bolus intravenous injection. The concentrations of the tracer candidate in striatum (as the target tissue), thalamus (as the reference tissue), and plasma samples were measured through quantitative LC–MS/MS analysis with the MRM<sup>11</sup> (multiple reaction monitoring) transition as *m/z* 391.1 → 281.0 (e.g., 5, Figure 2A and Figure 2B). The lowest level of quantitation (LOQ) was 0.1 ng/g for brain tissues and 0.01 ng/mL for plasma samples.

Whereas all three candidates exhibited comparable in vitro profiles, their tracer candidacies were readily differentiated in vivo through our LC–MS/MS platform. In terms of target tissue specificity, both compounds 5 and 6 exhibited good striatum to thalamus ratios of 9.4 and 11.8, respectively, based on the AUC (area under the curve). Candidate 7 demonstrated a low ratio of 2.6. High striatal uptake was observed with compounds 5 and 7, both achieving greater than 1% injected dose per gram of tissue (% ID/g) at 10 min after injection, whereas the value was lower with compound 6 at 0.3% ID/g. As a result, 5 clearly emerged as the compound for advancement because it showed both high target tissue specificity and high target tissue uptake (Figure 2C and Figure 2D).

**Surface Plasmon Resonance (SPR) Binding Assay.** The LC–MS/MS results showed a steep drop of 5 concentration over time, suggesting fast in vivo kinetics. To better characterize the PDE10A binding properties of this molecule, we utilized a surface plasmon resonance (SPR) spectroscopy binding assay with purified truncated human PDE10A enzyme (amino acids 442–779) covalently attached to a CMS (carboxymethyl S) chip to measure affinity (*K<sub>D</sub>*), on-rate (*k<sub>a</sub>*), and off-rate (*k<sub>d</sub>*). Consistent with its PDE10A inhibition potency (IC<sub>50</sub> = 1.9 nM), 5 showed high affinity to PDE10A with a *K<sub>D</sub>* of 1.2 nM (Figure 3). This molecule exhibited fast on-rate (*k<sub>a</sub>* = 1.4 × 10<sup>8</sup> M<sup>-1</sup> s<sup>-1</sup>) and fast off-rate (*k<sub>d</sub>* = 1.7 × 10<sup>-1</sup> s<sup>-1</sup>). The derived *T*<sub>1/2</sub> was only 0.1 min. This fast off-rate in vitro supports the fast washout observed in Figure 2 above.

**In Vivo Saturable Binding and PDE10A *B<sub>max</sub>* Determination.** High saturable specific binding in target tissue is one requisite tracer characteristic for measurement of target–ligand interaction. To demonstrate saturable striatal uptake of the tracer candidate in vivo, 5 was administered at a range of dosages from 1 to 1000 μg/kg in rats by bolus intravenous injection. Striatal tissues, thalamic tissues, and blood samples

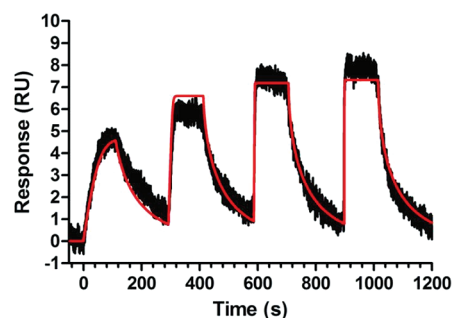


**Figure 3.** Biacore assay for *K<sub>D</sub>* determination. Unlabeled 5 was tested at 1000, 200, 40, and 8 nM. Kinetic titration experiments were performed by injecting the low to high inhibitor solutions at 2 min intervals onto the PDE10A chip surface (black trace, measured data; red trace, best fit to 1:1 binding model).

were collected at 10 min after dosing. Compound concentrations in the striatum and the thalamus were measured using LC–MS/MS. Specific striatum uptake was derived by subtraction of the tracer levels in the thalamus (as the reference tissue for nonspecific binding due to its low PDE10A expression level) from the levels in the striatum (as total binding due to its high PDE10A expression level) (Figure 4A). The resulting curve shape indicated that specific striatal binding of 5 was able to reach saturation in vivo. This study also enabled measurement of target density of PDE10A in the striatum showing a *B<sub>max</sub>* of 1.15 ± 0.11 pmol/mg (388.4 ± 38.4 ng/g) of wet tissue. The ED<sub>50</sub> (dosage to reach 50% of plateau) was determined by nonlinear regression to arrive at a value of 219.6 μg/kg. To derive target occupancy of 5, 100% target coverage was set as the maximum (plateau) value of striatal specific uptake. Plotting percent of target occupancy against the tracer concentration in the plasma (Figure 4B) revealed a plasma EC<sub>50</sub> of 101.8 ± 10.3 nM (53.2 ± 3 ng/mL).

**Characterization of in Vitro [<sup>3</sup>H]5 Binding to PDE10A Using Rat Striatal Homogenate.** Radiolabeled tracer, [<sup>3</sup>H]5, was utilized to perform *K<sub>D</sub>* and *B<sub>max</sub>* assessments on rat striatal homogenate. For comparison, nonspecific binding was calculated in two different ways: one using an excess of nonradiolabeled compound (Figure 5A), the other using [<sup>3</sup>H]5 bound to thalamus tissue (Figure 5B). Both approaches showed [<sup>3</sup>H]5 bound to striatal homogenates in a saturable manner. The binding affinity was calculated using nonlinear regression to an equilibrium dissociation constant (*K<sub>D</sub>*) of 0.94 nM. This is consistent with the value measured by the Biacore assay (*K<sub>D</sub>* = 1.2 nM). The *B<sub>max</sub>* of rat striatum tissue for PDE10A binding by [<sup>3</sup>H]5 was 2.1 pmol/mg of protein. The PDE10A target density in the striatum derived from in vitro homogenate binding data was consistent with target density derived from in vivo striatal binding using our LC–MS/MS technology. This comparison of nonspecific binding calculations further confirmed that thalamus was sufficient as the reference tissue to compare against target tissue binding in the striatum.

**In Vitro Binding Displacement.** To determine whether the tracer could be displaced, [<sup>3</sup>H]5 was studied in binding displacement experiments first with unlabeled 5 and then with a known selective and structurally distinct PDE10A inhibitor 17 (MP-10) (Figure 6). By use of the Cheng–Prusoff equation,<sup>12</sup> *K<sub>i</sub>* values were calculated for 5 (IC<sub>50</sub> = 3.47 nM and *K<sub>i</sub>* = 1.18 nM) and 17 (IC<sub>50</sub> = 0.50 nM and *K<sub>i</sub>* = 0.17 nM). The displacement of [<sup>3</sup>H]5 by the unlabeled 5 showed that the binding to PDE10A was competitive. Meanwhile, the displace-

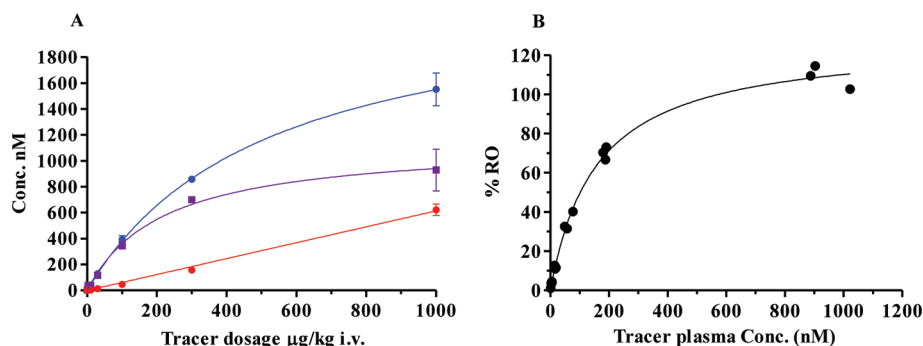


**Figure 4.** In vivo saturation binding of PDE10 by 5. Rats were intravenously administered 5 doses ranging from 1 to 1000  $\mu\text{g}/\text{kg}$ . At 10 min after injection, animals were euthanized and tissues were collected. The tracer concentration levels were determined using LC–MS/MS. (A) Saturable striatum specific uptake of 5. Blue circles represent striatum concentration as total binding. Red circles represent the thalamus concentration as nonspecific binding. Purple squares represent (STR-THA) specific binding. GraphPad Prism, version 5, software was used for nonlinear regression of the curve fit. Results are expressed as the mean  $\pm$  SEM (standard error of the mean),  $N = 4$  animals per group. (B) Correlation of the tracer plasma concentration with calculated target coverage (RO%). The plateau value of the striatum specific binding (STR-THA) was used as 100% of target occupancy.

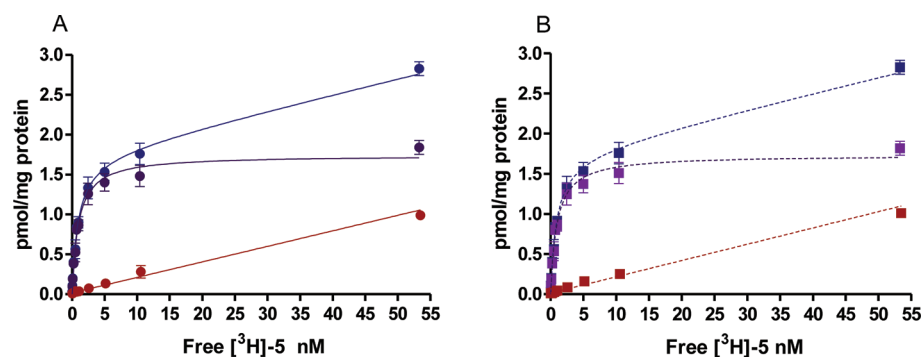


**Figure 5.** Saturation binding of [<sup>3</sup>H]5 in rat striatum homogenates for PDE10A target density ( $B_{\text{max}}$ ) and the apparent affinity ( $K_{\text{D}}$ ) determination using two nonspecific binding calculations. Saturation binding was determined by incubating rat striatum homogenates with concentrations of [<sup>3</sup>H]5 ranging from 0.01 to 50 nM in a final volume of 200  $\mu\text{L}$ . (A) Nonspecific binding was determined using an excess (1  $\mu\text{M}$ ) of unlabeled compound. Blue circles represent total binding. Red circles represent nonspecific binding, and purple circles represent specific binding. (B) Nonspecific binding was defined as [<sup>3</sup>H]5 binding to thalamic tissue homogenate. Blue squares indicate total binding. Red squares indicate nonspecific binding ([<sup>3</sup>H]5 binding to thalamic tissue homogenate), and purple squares indicate specific binding. GraphPad Prism, version 5, software was used for the nonlinear regression of the curve fit. Data are presented as the mean  $\pm$  SEM. Error bars in the graph represent  $N = 4$  data points.

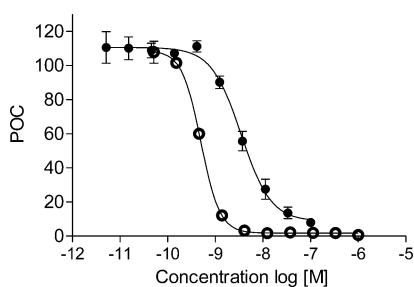


**Figure 6.** [<sup>3</sup>H]5 binding displacement with a selective PDE10A inhibitor. The dose–response curves of various PDE10A inhibitors were determined in competition binding studies using native striatum tissue homogenates with the concentration of [<sup>3</sup>H]5 at approximately the  $K_{\text{D}}$  in the presence of increasing concentrations of displacer compound from 5 pM to 100 nM. Open circles represent 17, and filled circles represent 5. Curves were analyzed using nonlinear regression on GraphPad Prism. Results are expressed as the mean  $\pm$  SEM (standard error of mean), and error bars in the graph represent  $N = 2$  per data point. The  $K_{\text{i}}$  values were calculated for 17 ( $\text{IC}_{50} = 0.50$  nM and  $K_{\text{i}} = 0.17$  nM) and the 5 ( $\text{IC}_{50} = 3.47$  nM and  $K_{\text{i}} = 1.18$  nM).

ment of [<sup>3</sup>H]5 by 17, a structurally distinct and potent PDE10A inhibitor, indicated that the tracer is not scaffold

specific and can be used to measure target occupancy of other PDE10A inhibitors binding to the same active site.

**Ex Vivo Autoradiography of [<sup>3</sup>H]5 Distribution in Rat Brain.** To visualize the distribution of 5 in the brain in vivo, rats ( $n = 3–4$  per group) were dosed with 3, 10, 30, or 100  $\mu\text{Ci}$  [<sup>3</sup>H]5 via a jugular vein catheter and brains were collected 10 min after dosing. The best signal-to-noise ratio of  $>3$  was obtained with 30  $\mu\text{Ci}$  (not shown). Therefore, a subsequent set of rats ( $n = 3–4$  per group) was dosed with vehicle or 10 mg/kg 17 and 30  $\mu\text{Ci}$  [<sup>3</sup>H]5 was administered via a jugular vein catheter after 50 min. Brains were collected 10 min after tracer injection, and sagittal brain sections ( $n = 4$  per brain) were analyzed using real-time autoradiography. Radioactive uptake was the highest in the striatum, and very low binding was detectable in other brain regions including the thalamus (Figure 7A). The binding pattern of [<sup>3</sup>H]5 in vivo was consistent with the published results.<sup>3</sup> Striatum and thalamus were selected as regions of interest, and binding was measured as counts/ $\text{mm}^2$  using M3vision (Biospace, Paris, France). Specific striatal binding was determined by subtracting thalamus binding from striatum and blocked by pre-dosing with 17 by an average of 74% (Figure 7B).

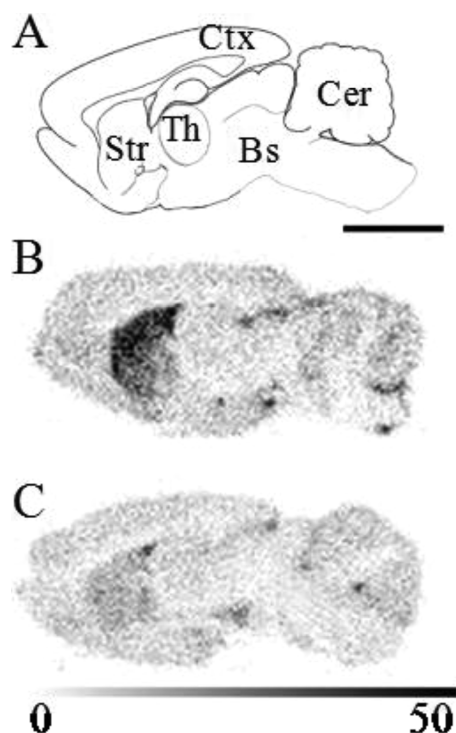


**Figure 7.** Visualization of in vivo PDE10A binding and occupancy by 17 by autoradiography with  $[^3\text{H}]\mathbf{5}$ . (A) Diagram of sagittal section of rat brain which indicates the areas of autoradiography results: Ctx, cortex; Th, thalamus; Str, striatum; Bs, brain stem; Cer, cerebellum. (B) Representative autoradiograph of a sagittal section from a rat dosed with vehicle and 30  $\mu\text{Ci}$   $[^3\text{H}]\mathbf{5}$  showing high binding in the striatum and only low binding in other brain areas. (C) Representative autoradiograph of a sagittal section from a rat dosed with 17 (10 mg/kg po, 60 min) and 30  $\mu\text{Ci}$   $[^3\text{H}]\mathbf{5}$ , demonstrating a strong blockade of uptake in the striatum. Color bar represents counts, and scale bar represents 5 mm.

**In Vivo Measurement of Target Occupancy.** To demonstrate the full utility of  $\mathbf{5}$ , we performed PDE10A occupancy studies in vivo in rats with 17 using the LC–MS/MS technology. Blocker 17 was administered orally with dosages 1, 3, 10, and 30 mg/kg. Tracer  $\mathbf{5}$  (6  $\mu\text{g}/\text{kg}$ ) was injected intravenously at 50 min after 17 dosing. The dosage of the tracer was chosen to occupy less than 5% of the target, sufficient to generate reliable signal values for the binding potential (BP) calculation.<sup>8</sup> Ten minutes later, samples from blood, striatum, and thalamus were collected. Using LC–MS/MS analysis, we obtained blocker 17 exposure levels in the plasma and striatum (Figure 8A) and obtained tracer  $\mathbf{5}$  exposure levels in the target tissue (striatum), reference tissue (thalamus), and plasma (Figure 8B). The maximum striatal PDE10A occupancy by 17 at 30 mg/kg was 91.2%. Also noteworthy was that target occupancy by 17 at 10 mg/kg was 83.8%, comparable to the occupancy of 74% measured by  $[^3\text{H}]\mathbf{5}$  with autoradiography. The  $\text{ED}_{50}$  of 17 to occupy PDE10A in the striatum was measured with a value of  $2.3 \pm 0.3$  mg/kg (Figure 8C). The target coverage of 17 was also plotted against plasma and striatum exposure levels to obtain the  $\text{EC}_{50}$  values of  $241.5 \pm 36.1$  nM and  $639.7 \pm 69.1$  nM, respectively. This experiment confirmed that  $\mathbf{5}$  is a useful tracer for measurement of target occupancy of PDE10A inhibitors in vivo.

## CONCLUSION

Using a combination of stringent selection criterion and the LC–MS/MS technology to screen unlabeled tracer candidates in rodents, we rapidly identified a promising PDE10A tracer  $\mathbf{5}$  based on in vivo evaluation of three nonradiolabeled PDE10A tracer candidates with similarly promising in vitro characteristics, bypassing the traditionally cost and time prohibitive requirement of radiolabeling tracer candidates prior to in vivo tracer profiling. Tracer  $\mathbf{5}$  exhibited the superior in vivo profile, with high affinity, high specificity (good striatum to thalamus or target to reference ratio), and good striatum uptake. The in vitro and in vivo features of this molecule were extensively characterized using both the unlabeled  $\mathbf{5}$  and the  $[^3\text{H}]\mathbf{5}$ . By use of ex vivo autoradiography,  $[^3\text{H}]\mathbf{5}$  was used to assess relative expression levels of PDE10A in rat brain tissues and target occupancy of 17. Using LC–MS/MS technology, we demonstrated the utility of  $\mathbf{5}$  by measuring the in vivo PDE10A target occupancy of 17. These results further suggested that  $\mathbf{5}$  could possess suitable characteristics to be a PET imaging tracer similar to other PDE10A PET tracers reported to date.<sup>13</sup> Our findings on advancing  $\mathbf{5}$  as a PET tracer candidate will be reported in a separate publication.

## EXPERIMENTAL SECTION

**Chemistry, Materials, and General Methods.** Unless otherwise noted, all reagents and solvents were obtained from commercial suppliers such as Aldrich, Sigma, Fluka, Acros, EDM Sciences, etc. and used without further purification. Dry organic solvents (dichloromethane, acetonitrile, DMF, etc.) were purchased from Aldrich packaged under nitrogen in Sure/Seal bottles. All reactions involving air or moisture sensitive reagents were performed under a nitrogen or argon atmosphere. Silica gel chromatography was performed using prepacked silica gel cartridges (Biotage or RediSep). Microwave assisted reactions were performed in Biotage Initiator Sixty microwave reactor.  $^1\text{H}$  NMR spectra were recorded on a Bruker DRX 300 MHz, Bruker DRX 400 MHz, Bruker AV 400 MHz, Varian 300 MHz, or a Varian 400 MHz spectrometer at ambient temperature. Chemical shifts are reported in parts per million (ppm,  $\delta$  units). Data are reported as follows: chemical shift, number of protons, multiplicity ( $s$  = singlet,  $d$  = doublet,  $t$  = triplet,  $q$  = quartet,  $br$  = broad,  $m$  = multiplet), coupling constants, and number of protons. Reactions were monitored using Agilent 1100 series LC/MSD SL high performance liquid chromatography (HPLC) systems with UV detection at 254 nm and a low resonance electrospray mode (ESI). All final compounds were purified to >95% purity, as determined by high performance liquid chromatography (HPLC). HPLC methods used the following: Agilent 1100 spectrometer, Zorbax SB-C18 column (50 mm  $\times$  3.0 mm, 3.5  $\mu\text{m}$ ) at 40  $^\circ\text{C}$  with a 1.5 mL/min flow rate; solvent A of 0.1% TFA in water, solvent B of 0.1% TFA in MeCN; 0.0–3.0 min, 5–95% B; 3.0–3.5 min, 95% B; 3.5–3.51 min, 5% B. Flow from UV detector was split (50:50) to the MS detector, which was configured with API-ES as ionizable source. All high resolution mass spectrometry (HRMS) data were acquired on a Synapt G2 HDMS instrument (Waters Corporation, Manchester, U.K.) operated in positive electrospray ionization mode. The sample was diluted to 10  $\mu\text{M}$  in 50% acetonitrile (v/v), 0.1% formic acid (v/v) and infused into the mass spectrometer at a flow rate of 5  $\mu\text{L}/\text{min}$  through an electrospray ionization source operated with a capillary voltage of 3 kV. The sample cone was operated at 30 V. The time-of-flight analyzer was operated at a resolution (fwhm) of 30 000 at  $m/z$  785 and was calibrated over the  $m/z$  range 50–1200 using a 1  $\mu\text{M}$  sodium iodide (NaI) solution (50% v/v acetonitrile solution). To obtain accurate mass measurements, an internal lock-mass correction was applied using leucine enkephalin ( $m/z$  556.2771). Collision induced fragmentation (CID) was performed using an injection voltage of 28 V. Instrument control was performed through the software suite MassLynx, version 4.1.

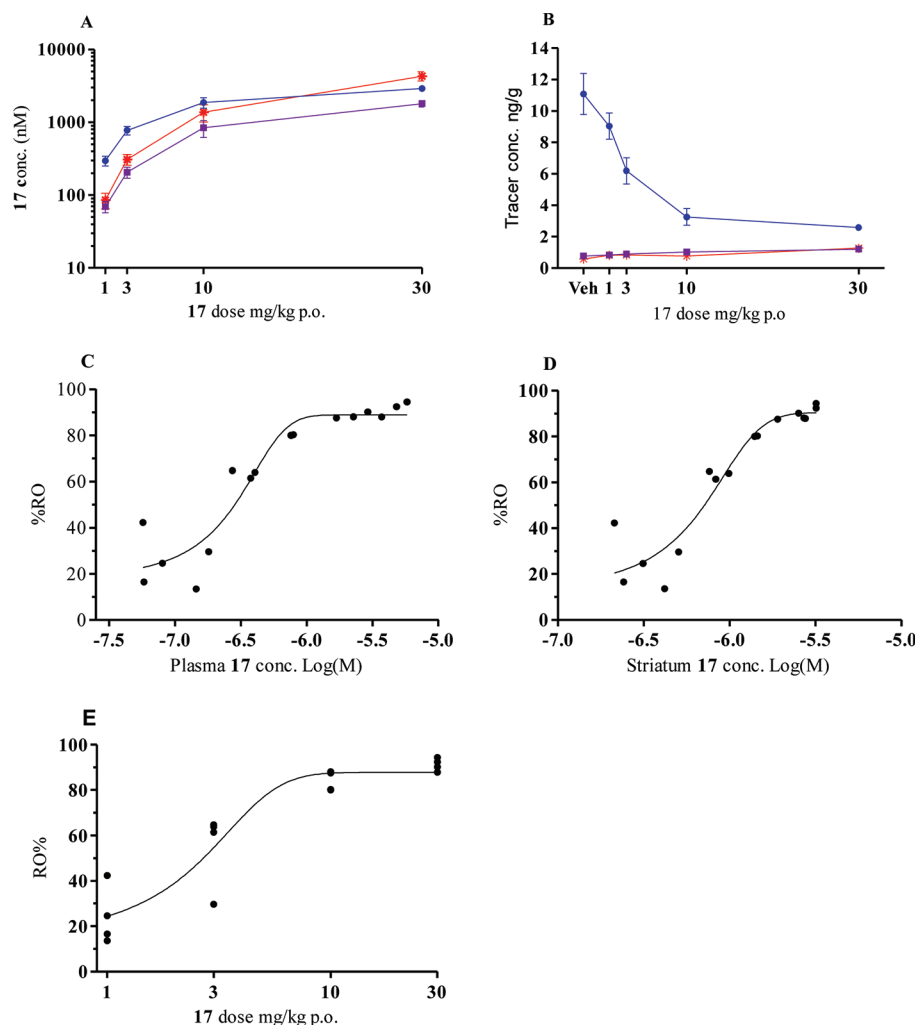


**Figure 8.** Determination of in vivo PDE10A occupancy of 17 using tracer 5. Both the blocker 17 concentration and tracer 5 concentrations in the plasma, striatum, and thalamus tissues were measured by LC–MS/MS from the same sample preparation. (A) 17 exposure levels in the plasma (red asterisks), striatum (blue circles), and thalamus (purple squares) at 1 h after oral dosing. (B) 5 concentrations in the plasma (red asterisks), striatum (blue circles), and thalamus (purple squares) were plotted against the 17 dosages. (C–E) 17 target occupancy in the striatum was plotted against 17 dosages, exposure levels in the plasma, and exposure levels in the striatum, respectively, to calculate  $ED_{50}$  and  $EC_{50}$  in plasma and striatum. Curves were analyzed using nonlinear regression on GraphPad Prism. Results in parts A and B are expressed as the mean  $\pm$  SEM (standard error of the mean), and error bars in graph represent  $N = 4$  animals per dosage group.

**Compounds.** Tritium-labeled compound [ $^3H$ ]5 was synthesized by Moravek Biochemicals, Inc., with a specificity of 45 Ci/mmol (in ethanol solution) and 99.5% purity as analyzed by HPLC.

**6,7-Dimethoxycinnolin-4-ol (2).** 2'-Amino-4',5'-dimethoxyacetophenone (15.82 g, 81.0 mmol) was solubilized in concentrated HCl (460 mL) and water (80 mL). The temperature was cooled to  $-5\text{ }^{\circ}\text{C}$  using ice/brine bath, and the resulting mixture was stirred vigorously. A solution of sodium nitrite (5.67 g, 81.8 mmol) and water (29.2 mL, 1621 mmol) was added to the reaction mixture over 1 h. The mixture was allowed to continue to stir for 1 h. Then the temperature was raised to  $60\text{ }^{\circ}\text{C}$ . After heating for 4 h, the solution was allowed to cool to room temperature. The solid was filtered and collected. The solid was transferred to a rbf and suspended with deionized water. The pH was adjusted to  $\sim 12$  by adding NaOH. The solution was then neutralized with concentrated HCl. A precipitate was formed and filtered to produce desired intermediate 2 (13.78 g, 82.5% yield).  $^1H$  NMR (300 MHz, DMSO):  $\delta$  ppm 3.88 (s, 6H), 6.94 (s, 1H), 7.31 (s, 1H), 7.62 (s, 1H), 13.35 (s, 1H). LC–MS: ( $m + 1 = 207.1$ ). Material was carried to the next step without further purification.

**4-Bromo-6,7-dimethoxycinnoline (3).** To a 150 mL round-bottomed flask were added 6,7-dimethoxycinnolin-4-ol (2.0049 g, 9.723 mmol) and phosphorus oxybromide (1.387 mL, 13.61 mmol)

with 40 mL of chloroform. The reaction mixture was allowed to stir at  $65\text{ }^{\circ}\text{C}$  for 3.5 h. The mixture was allowed to cool to room temperature, and the volatile solvent was removed by vacuum. The solid residue was then poured onto ice, and to it was added saturated  $\text{NaHCO}_3$ . The aqueous mixture was filtered to collect the solid. The solid was placed in a rbf and triturated with 4 mL of DCM and 20 mL of hexane. The solid was filtered and dried by vacuum. The solid was recrystallized in hot MeOH to afford desired intermediate 3 (1.63 g, 62.3% yield).  $^1H$  NMR (300 MHz, DMSO):  $\delta$  ppm 4.05 (s, 6H), 7.22 (s, 1H), 7.79 (s, 1H), 9.40 (s, 1H). LC–MS: ( $m + 1 = 269.0$ ).

**4-(6-Fluoro-5-methylpyridin-3-yl)-6,7-dimethoxycinnoline (4).** To a round-bottomed flask were added 3 (0.6372 g, 2.4 mmol), 6-fluoro-5-methylpyridin-3-ylboronic acid (0.4094 g, 2.6 mmol), palladium tetrakis(triphenylphosphine) (0.1525 g, 0.12 mmol), and cesium carbonate (2.1 g, 6.4 mmol) in DME (250 mL) and water (10 mL). The mixture was stirred at  $80\text{ }^{\circ}\text{C}$  overnight. The reaction mixture was diluted with water and extracted with EtOAc. The organic extract was washed with water, saturated NaCl, dried over  $\text{MgSO}_4$ , filtered, and concentrated in vacuo. The solid was allowed to stir in ether for 15 min and was filtered. The solid was dried by vacuum to afford the desired intermediate 4 (0.46 g, 65% yield). LC–MS shows product peak at 4.852 min ( $m + 1 = 300.1$ ).  $^1H$  NMR (300 MHz, chloroform-

d):  $\delta$  ppm 2.44 (s, 3 H), 3.95 (s, 3 H), 4.14 (s, 3 H), 6.99 (s, 1 H), 7.80 (dd,  $J = 9.21, 1.61$  Hz, 1 H), 7.84 (s, 1 H), 8.26 (s, 1 H), 9.02 (s, 1 H).

**5-(6,7-Dimethoxycinnolin-4-yl)-*N*-isopropyl-3-methylpyridin-2-amine (5).** In a glass microwave reaction vessel were placed 4 (0.0545 g, 0.18 mmol) and isopropylamine (0.156 mL, 1.8 mmol) in DMSO (2 mL), and the mixture was stirred at 90 °C overnight. The crude product was adsorbed onto a plug of silica gel and chromatographed through a Biotage prepacked silica gel column (40S), eluting with a gradient of 1–5% MeOH in CH<sub>2</sub>Cl<sub>2</sub> over 20 column volumes to provide 5 (0.0438 g, 71% yield, 99% purity). LC–MS product peak was found at 2.8 min ( $m + 1 = 339.2$ ). <sup>1</sup>H NMR (300 MHz, chloroform-*d*):  $\delta$  ppm 1.38 (d,  $J = 6.28$  Hz, 6 H), 2.24 (s, 3 H), 4.00 (s, 3 H), 4.16 (s, 3 H), 4.31 (d,  $J = 7.16$  Hz, 1 H), 4.38–4.53 (m, 1 H), 7.30 (s, 1 H), 7.49 (s, 1 H), 7.83 (s, 1 H), 8.32 (s, 1 H). HRMS (ES+) calculated for [C<sub>19</sub>H<sub>22</sub>N<sub>4</sub>O<sub>2</sub>]<sup>+</sup>: 338.404. Found: 338.174.

**(*S* or *R*)-5-(6,7-Dimethoxycinnolin-4-yl)-3-methyl-*N*-(1-(pyridin-2-yl)propan-2-yl)pyridin-2-amine (6).** A mixture of 4 (200 mg, 0.67 mmol), 1-(pyridin-2-yl)propan-2-amine (140 mg, 1.0 mmol), and DMSO (2 mL) was heated at 120 °C for 18 h. The resulting solution was purified by preparative HPLC (10–60% CH<sub>3</sub>CN/H<sub>2</sub>O/0.1%TFA) to give a mixture of isomers as the TFA salts (235 mg). Chiral separation of the isomers was performed on Berger Multigram II SFC (supercritical fluid chromatography) using a Chiralcel AS-H (250 mm × 21 mm, 5  $\mu$ m) column with 80% liquid CO<sub>2</sub> and 20% methanol with 0.2% DEA (diethylamine) as the mobile phase and flow rate of 65 mL/min at 40 °C. The desired compound 6 was the second eluting compound, and it was isolated in 33 mg yield (0.077 mmol) with >99% enantiopurity. Enantiopurity of 6 was determined on an analytical SFC/MS instrument using a Chiralpak AS-H (150 mm × 4.6 mm, 5  $\mu$ m) with 80% liquid CO<sub>2</sub> and 20% methanol with 0.2% DEA (diethylamine) as the mobile phase and flow rate of 4.0 mL/min at 40 °C. Absolute stereochemistry was not determined. <sup>1</sup>H NMR (400 MHz, MeOH-*d*):  $\delta$  ppm 9.20 (1 H, s), 8.79 (1 H, dd,  $J = 5.8, 0.9$  Hz), 8.49 (1 H, td,  $J = 7.9, 1.6$  Hz), 8.35 (1 H, d,  $J = 2.0$  Hz), 8.07 (1 H, d,  $J = 8.0$  Hz), 7.95–8.01 (1 H, m), 7.87–7.94 (1 H, m), 7.79 (1 H, s), 7.44 (1 H, s), 4.76–4.88 (1 H, m), 4.17 (3 H, s), 4.10 (3 H, s), 3.43–3.64 (2 H, m), 2.37 (3 H, s), 1.49 (3 H, d,  $J = 6.7$  Hz). HRMS (ES+) calcd for [C<sub>24</sub>H<sub>26</sub>N<sub>5</sub>O<sub>2</sub>]<sup>+</sup>: 415.488. Found: 415.201.

***N*-(2,2-Difluoroethyl)-5-(6,7-dimethoxycinnolin-4-yl)-*N*-ethyl-3-methylpyridin-2-amine (7).** In a glass microwave reaction vessel were placed 4 (0.0555 g, 0.195 mmol) and 2,2-difluoroethanamine (0.1609 g, 1.95 mmol) in DMSO (2 mL), and the mixture was stirred at 90 °C. The solution was allowed to stir for 2 days. The reaction mixture was diluted with water and extracted with EtOAc. The organic extract was washed with water, saturated NaCl, dried over MgSO<sub>4</sub>, filtered, and concentrated in vacuo. The crude product was adsorbed onto a plug of silica gel and chromatographed through a Biotage prepacked silica gel column (40S), eluting with a gradient of 1–5% MeOH in CH<sub>2</sub>Cl<sub>2</sub>, to provide *N*-(2,2-difluoroethyl)-5-(6,7-dimethoxycinnolin-4-yl)pyridin-2-amine (0.0308 g, 45.7% yield, 97.9% purity). LC–MS product peak was found at 4.174 min ( $m + 1 = 347.1$ ). <sup>1</sup>H NMR (300 MHz, DMSO-*d*<sub>6</sub>):  $\delta$  ppm 3.30 (d,  $J = 7.16$  Hz, 3 H), 3.80 (td,  $J = 15.60, 4.02$  Hz, 1 H), 3.99–4.07 (m, 6 H), 6.81 (d,  $J = 8.62$  Hz, 1 H), 7.19 (s, 1 H), 7.76 (s, 1 H), 7.82 (dd,  $J = 8.70, 2.41$  Hz, 1 H), 8.35 (d,  $J = 1.90$  Hz, 1 H), 9.03 (s, 1 H).

To a round-bottomed flask were added *N*-(2,2-difluoroethyl)-5-(6,7-dimethoxycinnolin-4-yl)pyridin-2-amine (0.0625 g, 0.18 mmol) and sodium hydride (0.0052 mL, 0.20 mmol) in DMF (10 mL). The mixture was allowed to stir for 10 min, and iodoethane (0.030 mL, 0.36 mmol) was added. The mixture was stirred overnight. The reaction mixture was diluted with water and extracted with EtOAc. The organic extract was washed with water, saturated NaCl, dried over MgSO<sub>4</sub>, filtered, and concentrated in vacuo. The crude product was adsorbed onto a plug of silica gel and chromatographed through a Biotage prepacked silica gel column (40S), eluting with a gradient of 1–5% MeOH in CH<sub>2</sub>Cl<sub>2</sub> to provide 7 (0.0327 g, 48% yield, 99% purity). LC–MS product peak was found at 5.223 min ( $m + 1 = 375.2$ ). <sup>1</sup>H NMR (300 MHz, chloroform-*d*):  $\delta$  ppm 1.30 (t,  $J = 7.09$

Hz, 3 H), 3.64 (q,  $J = 7.02$  Hz, 2 H), 3.89–4.07 (m, 5 H), 4.13 (s, 3 H), 6.78 (d,  $J = 8.48$  Hz, 1 H), 7.18 (s, 1 H), 7.72 (dd,  $J = 8.77, 2.48$  Hz, 1 H), 7.80 (s, 1 H), 8.39 (d,  $J = 1.90$  Hz, 1 H), 9.02 (s, 1 H). HRMS (ES+) calculated for [C<sub>19</sub>H<sub>20</sub>F<sub>2</sub>N<sub>4</sub>O<sub>2</sub>]<sup>+</sup>: 374.385. Found: 374.155.

**1-(4-Fluoro-5-methoxy-2-nitrophenyl)ethanone (9).** A 2 L three-neck round-bottom flask equipped with an overhead stirrer, addition funnel with nitrogen inlet, and thermocouple was charged with 8 (54.06 g, 321 mmol) and acetic anhydride (220 mL). The resulting solution was cooled with an ice/water bath. Nitric acid (70% a.c.s, 43.4 mL, 964 mmol) was added dropwise over 30 min. At the end of the addition, the cooling bath was removed and stirring was continued at room temperature. After ~18 h of stirring, the reaction mixture was heated to an internal temperature of 45 °C for 1 h and 20 min. Heating was stopped, and the reaction mixture was cooled to internal temperature of 3 °C. The solid that formed was isolated by filtration, washed with ice cold water, and dried. The filtrates were carefully combined and allowed to stand at an internal temperature of 7 °C for 30 min. A second batch of solids were isolated by filtration and dried. The filtrate was partitioned between water and ethyl acetate. The water layer was extracted with EtOAc, and the organic layer was washed with an aqueous saturated NaHCO<sub>3</sub> solution, dried over MgSO<sub>4</sub>, filtered, and concentrated in vacuum. Purification was by MPLC (hexanes/EtOAc, 100/0 to 90/10, then 80/20). The isolated product plus the solids collected by filtration combined gave the desired intermediate 9 (68.5 g, 82% yield). <sup>1</sup>H NMR (400 MHz, DMSO-*d*<sub>6</sub>):  $\delta$  ppm 8.15 (d,  $J = 10.96$  Hz, 1 H), 7.46 (d,  $J = 8.22$  Hz, 1 H), 4.01 (s, 3 H), 2.55 (s, 3 H).

**1-(2-Amino-4-fluoro-5-methoxyphenyl)ethanone (10).** A 1 L three-neck round-bottom flask with mechanical stirrer, nitrogen inlet, and thermocouple was charged with 9 (13.8 g, 64.7 mmol), acetic acid (280 mL), and iron powder, where <10  $\mu$ m (18.08 g, 324 mmol) was added in one portion at room temperature. The resulting reaction mixture was heated at 100 °C internal temperature. Stirring was continued for 1.5 h. The reaction mixture was cooled to room temperature, filtered through a plug of Celite, and rinsed with EtOAc. The filtrate was concentrated in vacuo. Purification by MPLC (hexanes/EtOAc, 100/0 to 80/20) afforded the desired intermediate 10 (10.5 g, 89% yield). <sup>1</sup>H NMR (400 MHz, DMSO-*d*<sub>6</sub>):  $\delta$  ppm 7.37 (d,  $J = 9.68$  Hz, 1 H), 7.10 (br s, 2 H), 6.59 (d,  $J = 13.79$  Hz, 1 H), 3.78 (s, 3 H), 2.50 (s, 3 H).

**7-Fluoro-6-methoxycinnolin-4-ol (11).** Hydrochloric acid, 37% (1820  $\mu$ L, 21.84 mmol), was added to a cooled (ice/water) suspension of 10 (200 mg, 1.092 mmol) in water (4 mL). A solution of sodium nitrite (181 mg, 2.62 mmol) in water (1 mL) was then added dropwise at 0 °C. Stirring was continued for ~1 h at 0 °C. The cooling bath was removed, and the reaction mixture was stirred at 65 °C for 4 h. The reaction mixture was cooled with an ice bath. The yellow solid that formed upon cooling was isolated by filtration, washed with ice-cold water, and dried under high vacuum overnight to produce the desired intermediate 11 (192 mg, 91% yield). <sup>1</sup>H NMR (400 MHz, DMSO-*d*<sub>6</sub>):  $\delta$  ppm 13.57 (br s, 1 H), 7.71 (s, 1 H), 7.55 (d,  $J = 9.10$  Hz, 1 H), 7.45 (d,  $J = 11.35$  Hz, 1 H), 3.95 (s, 3 H).

**4-Bromo-7-fluoro-6-methoxycinnoline (12).** A suspension of 11 (2.6 g, 0.013 mol) in chloroform (30 mL) under nitrogen atmosphere was treated with phosphorus oxybromide (14.5 g, 0.0493 mol) and stirred at room temperature for 12 h. The mixture was then heated to reflux for 4 h. Reaction mixture was poured on crushed ice and extracted with ethyl acetate (3 × 100 mL). The combined organic extracts were washed with aqueous saturated sodium bicarbonate solution, dried over anhydrous sodium sulfate, and concentrated in vacuum. The crude mixture was then purified by silica gel column chromatography to afford the desired intermediate 12 (1.4 g, 41% yield) as a white solid. <sup>1</sup>H NMR (DMSO):  $\delta$  4.13 (s, 3H, OCH<sub>3</sub>), 7.43–7.45 (d, 1H, 2-Ar-H), 8.36–8.39 (d, 1H, 5-Ar-H), 9.58 (s, 1H, 3-Ar-H). TOF MS (ES+) 257.11/259.11.

**7-(Benzyloxy)-4-bromo-6-methoxycinnoline (13).** To a microwave vial was added 12 (1.0804 g, 4.2 mmol), benzyl alcohol (0.440 mL, 4.2 mmol), and LHMDS (1 M solution in THF, 6.3 mL, 6.3 mmol) in DMF. The resulting mixture was heated to 50 °C for 3 h.



The reaction mixture was allowed to cool to room temperature and then diluted with water (10 mL) and extracted with EtOAc (3 × 10 mL). The organic extract was washed with water (3 × 10 mL), saturated NaCl solution, dried with magnesium sulfate, filtered, and concentrated. The crude product was adsorbed onto a plug of silica gel and chromatographed through a Biotage prepacked silica gel column (40M), eluting with a gradient of 0.5–2.5% MeOH in dichloromethane to provide desired intermediate **13** (0.6807 g, 47% yield). LC–MS: [*m* + 1] = 345.2 with purity of 96.7%. <sup>1</sup>H NMR (300 MHz, CDCl<sub>3</sub>): δ ppm 4.11 (s, 3 H), 5.37 (s, 2 H), 7.23 (s, 1 H), 7.30–7.47 (m, 3 H), 7.48–7.57 (m, 2 H), 7.78 (s, 1 H), 9.25 (s, 1 H).

**7-(Benzyloxy)-4-(6-fluoro-5-methylpyridin-3-yl)-6-methoxycinnoline (14)**. In a microwave vessel were added **13** (0.6807 g, 1.972 mmol), 6-fluoro-5-methylpyridin-3-ylboronic acid (0.3095 g, 1.998 mmol), *trans*-dichlorobis(triphenylphosphine)palladium(II) (0.1087 g, 0.1578 mmol), and an aqueous solution of sodium carbonate (0.1937 mL, 3.944 mmol) in DME at 80 °C. The mixture was stirred overnight. The mixture was allowed to cool to room temperature, diluted with water (10 mL), and extracted with DCM (3 × 10 mL). The organic extract was washed with water (3 × 10 mL), saturated NaCl solution, dried with magnesium sulfate, filtered, and concentrated. The residue was filtered through a plug of silica to produce intermediate **14** which was directly advanced to the next step.

**4-(6-Fluoro-5-methylpyridin-3-yl)-6-methoxycinnolin-7-ol (15)**. To a suspension of **14** (355 mg, 946 μmol) in EtOH was added palladium on carbon (403 mg, 378 μmol). Hydrogen was bubbled through solution. Then the flask was flushed with hydrogen (3×), and the mixture was stirred overnight at room temperature. The resulting mixture was filtered through Celite, rinsing with DCM. Reverse phase purification was performed to produce the desired intermediate **15** which was directly taken to the next step. LC–MS: 286.0 [*M* + *H*], >99% purity.

**4-(6-Fluoro-5-methylpyridin-3-yl)-6,7-[<sup>3</sup>H]-dimethoxycinnoline (16)**. To a solution of **15** (8 mg, 28 μmol) in dimethylformamide, 1.1 mL, was added potassium carbonate (12 mg, 90 μmol). The resulting mixture was stirred for 10 min. Tritiated methyl iodide (CT<sub>3</sub>I, 50 μmol, 2500 mCi) was distilled over the vacuum line. The mixture was stirred at room temperature overnight. The reaction mixture was evaporated to dryness and purified by Gilson HPLC (Supelco SDC-18 column, 250 mm × 21.2 mm, 5 μm), eluting with a mobile phase of 40% acetonitrile in water with 0.1% TFA and a flow rate of 6 mL/min. UV detection was performed at 260 nm. The radiolabeled product **16** was collected after 22 min. Analytical HPLC to determine radiochemical purity was performed with a SpectraSYSTEM UV 1000 (SDC18 4.0 mm × 250 mm), with a flow rate of 1 mL/min. Mobile phases used were solvent A of water with 0.1% TFA and solvent B of acetonitrile with 0.1% TFA. Elution began at 0–10 min at 5% solvent B, 10–35 min at 5–100% B, then 35–40 min hold at 100% B. UV detection was performed at 254 nm. Compound **16** was synthesized with a decay corrected radiochemical yield of 4% and with a radiochemical purity of 99%.

**5-(6,7-[<sup>3</sup>H]Dimethoxycinnolin-4-yl)-*N*-isopropyl-3-methylpyridin-2-amine ([<sup>3</sup>H]**5**)**. To a solution of **16** (100 mCi) in dimethyl sulfoxide (200 μL) was added excess of isopropylamine (100 μL). The reaction mixture was heated to 90 °C overnight. The mixture was evaporated to dryness and purified by Discovery HPLC instrument (Supelco C-18 column, 250 mm × 21.2 mm, 5 μm), eluting with a mobile phase of 18% acetonitrile in water with 0.1% TFA and a flow rate of 5 mL/min. UV detection was performed at 254 nm. Analytical HPLC to determine radiochemical purity was performed with a SpectraSYSTEM UV 1000 (SDC18 4.0 mm × 250 mm), with a flow rate of 1 mL/min. Mobile phases used were solvent A of water with 0.1% TFA and solvent B of acetonitrile with 0.1% TFA. Elution began at 0–10 min at 5% solvent B, 10–35 min at 5–100% B, then 35–40 min hold at 100% B. UV detection was performed at 254 nm. The final 40 mCi of radiolabeled compound isolated was then formulated in ethanol at 1 mL/mCi. Compound [<sup>3</sup>H]**5** was synthesized with decay corrected radiochemical yield of 1.8% and with a radiochemical purity of 99%. The average specific radioactivity was found to be 46.7 Ci/mmol.

**Pharmacology. PDE10 Biochemical Assay.** Functional inhibition of human recombinant PDE10A was measured as described in the IMAP TR-FRET (time-resolved fluorescence energy transfer) assay kit protocol (Molecular Devices, Sunnyvale, CA, catalog no. R8160, R8176, or R8159). Compound was serially diluted in 100% DMSO from a 10 mM stock and further diluted in complete reaction buffer (10 mM Tris-HCl, pH 7.2, 10 mM MgCl<sub>2</sub>, 0.05% NaN<sub>3</sub>, 0.01% Tween 20, and 1 mM freshly added DTT) to a 4× concentration. Recombinant PDE10A enzyme and cAMP substrate were diluted in complete reaction buffer. The optimized binding buffer was 70% binding buffer A and 30% binding buffer B. Binding reagent (1:800) and terbium donor (1:400) were added to the binding buffer. All incubations were carried out at room temperature. Testing or control compounds (5 μL of each 4× concentration per well, 12-point dose–response curve ranging from 5.1 pM to 10 μM, tested in quadruplicate) were incubated with 5 μL of recombinant human PDE10A (0.06 units per well) in a 384-well microplate. After 30 min, 10 μL of cAMP substrate was added to each well for a final substrate concentration of 100 nM. After 1 h, 60 μL of binding buffer was added to each well. The plate was then incubated from 3 h to overnight before reading on an EnVision plate reader. The IMAP binding reagent binds to the nucleotide monophosphate generated from cyclic nucleotides (cAMP/cGMP) through phosphodiesterases and enables measurement of substrate turnover.

**Permeability and Transcellular Transport. Materials.** Digoxin and mannitol were purchased from Sigma-Aldrich (St. Louis, MO). [<sup>3</sup>H]Digoxin and [<sup>14</sup>C]mannitol were purchased from PerkinElmer Life and Analytical Sciences (Boston, MA). Transport buffer was prepared using Hank's balanced salt solution (HBSS) supplemented with 10 mM Hepes, pH 7.4, and 0.1% BSA (HBSS, Invitrogen, Grand Island, NY; BSA, bovine serum albumin, Calbiochem, La Jolla, CA).

**Cell Lines and Cultures.** Cultures were incubated at 37 °C in a humidified (95% relative humidity) atmosphere of 5% CO<sub>2</sub>/95% air. The parental cell line LLC-PK1 (porcine renal epithelial cells) was purchased from American Type Culture Collection (ATCC, Manassas, VA). Human MDR1 and Sprague-Dawley rat *mdr1a* transfectants in LLC-PK1 were generated at Amgen (Thousand Oaks, CA). Cells were cultured in medium 199 supplemented with 2 mM L-glutamine, penicillin (50 units/mL), streptomycin (50 μg/mL), and 10% (v/v) fetal bovine serum (all from Invitrogen).<sup>14</sup>

**Permeability and Transcellular Transport of Test Compounds.** LLC-PK1, MDR1-LLC-PK1, and *mdr1a*-LLC-PK1 cell monolayers were seeded onto porous (1.0 μm) polycarbonate 96-well transwell membrane filters (Millipore Corp., Billerica, MA) and cultured for 6 days with one medium replacement on day 4 prior to transwell experiments. Cells were washed once with warmed HBSS prior to transwell experiments. Experiments were initiated by replacing the buffer in each compartment with 0.15 mL of HBSS containing 0.1% BSA with and without 5 μM of test compound in triplicate wells. The plates were incubated for 2 h at 37 °C in an EVO incubator with shaking. Aliquots (100 μL) from both donor and receiver chambers were transferred to 96-well plates or scintillation vials. Protein was precipitated by addition of 200 μL of acetonitrile containing 0.1% formic acid and prazosin (25 ng/mL) as internal standard. After vortexing and centrifugation at 3000 rpm for 20 min, 150 μL supernatant samples were transferred to a new plate containing 50 μL water for LC–MS/MS analysis. Transcellular transport of [<sup>3</sup>H]digoxin was used as a positive control for Pgp. Paracellular permeability of [<sup>14</sup>C]mannitol was used to measure the integrity of the monolayer. Sample radioactivity was measured using a liquid scintillation counter (Packard Tri-Carb 2910TR, PerkinElmer).

The apparent permeability coefficient (*P*<sub>app</sub>) of all tested agents was estimated from the slope of cumulative amount (*dQ*) of the agent vs time (*dt*) and the following equation:

$$P_{app} = (dQ/dt)/(AC_0)$$

where *dQ/dt* is the penetration rate of the agent (μm/s), *A* is the surface area of the cell layer on the transwell (0.11 cm<sup>2</sup>), and *C*<sub>0</sub> is the initial concentration of the test compound (μM).

**Administration of Tracer Candidates in Rats and LC–MS/MS Detection.** *Animals.* All experiments were conducted under approved research protocols by Amgen's Animal Care and Use Committee (IACUC) and in accordance with National Institutes of Health Guide for Care and Use of Laboratory Animals in facilities accredited by the Association for the Assessment and Accreditation of Laboratory Animal Care (AALAC). Adult male Sprague-Dawley (SD) rats (250–280 g) were purchased from Harlan (Harlan, Indianapolis, IN). For the autoradiography experiments jugular vein catheters were inserted by the vendor. Rats were group-housed on a filtered, forced air isolation rack and maintained on sterile wood chip bedding in a quiet room on a 12 h light–dark cycle, with food and water available ad libitum. Animals were allowed a minimum of 3 days of adaptation to the laboratory conditions prior to being utilized in the experiments.

*Methods.* The tracer candidates were formulated in 20% Captisol, pH 4, with methanesulfonic acid (MSA). The tracer was administered by bolus intravenous injection via lateral tail vein. Animals were euthanized by decapitation under anesthetized conditions at different postdosing time points. Blood was collected and discrete brain areas (striatum, and thalamus) were rapidly dissected. The brain tissues were collected with preweighed flat-bottom 2 mL tubes, and the amount of tissue collected in each tube was weighed and calculated. The samples were snap frozen on dry ice and stored at  $-80^{\circ}\text{C}$  until use. Then 20% w/v of HPLC graded water was added to the sample tubes and samples were homogenized with an acoustic homogenizer (E210 Covaris, Inc.). Covaris settings were as follows:  $4^{\circ}\text{C}$ , duty cycle 20%, intensity 8, cycles per burst 500, treatment time  $6 \times 10$  s. Then 50  $\mu\text{L}$  of homogenate was transferred to a new tube and 10  $\mu\text{L}$  of methanol and 150  $\mu\text{L}$  of acetonitrile were added followed by extraction and centrifugation. The supernatant was transferred to well autosampler plate, and 150  $\mu\text{L}$  of HPLC grade water was added and mixed. The compound concentrations in the brain and plasma samples were analyzed employing high performance liquid chromatography (HPLC) coupled with triple quad mass spectrometry (API 4000, Applied Biosystem). The HPLC system employed a Waters Atlantis column.

*Surface Plasmon Resonance (SPR) Spectroscopy Binding Assay.* SPR measurements were performed on a Biacore T100 (GE Healthcare). His-PDE10A (442-779) was generated in-house; all other reagents were purchased from GE Healthcare or Sigma-Aldrich. PDE10 ( $\sim 3000$  RU) was coupled to the CMS chip using standard amine coupling. The immobilization running buffer consisted of 10 mM Hepes, pH 7.4, with 150 mM NaCl. Immobilization steps consisted of a 7 min EDC/NHS activation step [200 mM 1-ethyl-3-(3-dimethylaminopropyl)carbodiimide hydrochloride, 50 mM *N*-hydroxysuccinimide], 0.2 min of 20  $\mu\text{g}/\text{mL}$  PDE10A in 10 mM MES, pH 6.0, and 7 min of 1 M ethanolamine hydrochloride, pH 8.5.

Binding kinetics were measured with a 20 mM Tris-HCl buffer (pH 7.5) containing 50 mM NaCl, 5 mM  $\text{MgCl}_2$ , and 2% (v/v) DMSO. Stock solution of 5 was prepared at 10 mM in DMSO and diluted with running buffer to 1  $\mu\text{M}$ , 0.2  $\mu\text{M}$ , 40 nM, and 8 nM. Kinetic titration experiments<sup>15</sup> were performed by injecting the low to high compound solutions in 2 min intervals onto the PDE10A surface. All experiments were performed at  $25^{\circ}\text{C}$ .

The data were processed and analyzed using the T100 evaluation software and the CLAMP analysis software package (Center for Biomolecular Interactions, University of Utah, Salt Lake City, UT). The sample response was baseline corrected by subtracting reference flow cell data to correct for systematic noise and baseline drift. The response from blank injections was used to double-reference the binding data. The kinetic parameters were established by fitting the data to a 1:1 binding model which included a mass transfer limitation term.

*$K_D$  and  $B_{\text{max}}$  Measurement Using Rat Striatal Homogenate.* Brain homogenates were prepared from SD rat striatum and thalamus regions. Brain samples were weighed and 20% w/v of PDE10 homogenization buffer (50 mM Tris-HCl, pH 7.5, 1.2 mM  $\text{MgCl}_2$ , 0.1 mM DTT, 10% sucrose, 1 $\times$  Roche complete protease inhibitor mix) was added, followed by homogenization using an acoustic homogenizer (E210 Covaris, Inc.). The brain homogenate was then centrifuged at 4200g to pellet unbroken cells and nuclei. The

supernatant was collected and protein concentration of the total brain homogenate was determined using Biorad DC protein concentration assay. An amount of 20  $\mu\text{g}$  of homogenate protein of rat striatum and thalamus was added per well.

Brain homogenates were incubated with tritium labeled compound (with concentrations from 0.01 to 50 nM in a final volume of 200  $\mu\text{L}$ ). Nonspecific binding was determined using excess nonlabeled compound (1  $\mu\text{M}$ ) in assay buffer (50 mM Tris-HCl, pH 7.5, 5 mM  $\text{MgCl}_2$ , 1 $\times$  Roche complete protease inhibitor mix) for 1 h at room temperature. The binding reaction was terminated by rapid filtration through GF/C filter, and the mixture was presoaked in 0.3% PEI for 30 min and immediately rinsed 6 times with  $4^{\circ}\text{C}$  wash buffer (50 mM Tris-HCl, pH 7.5, 10 mM  $\text{MgCl}_2$ ). The filter plates were dried in a vacuum oven at  $56^{\circ}\text{C}$  for approximately 40 min, and 50  $\mu\text{L}$  of Microscint-20 was added per well. Plates were sealed and read on a Packard TopCount NXT plate reader for 2 min/well. Specific binding was calculated as total (cpm) minus nonspecific (cpm) binding.

Data were analyzed by nonlinear regression analysis using GraphPad Prism software, version 5 (GraphPad Inc., San Diego, CA), which fitted binding curves to the following equation for saturation binding experiments:

$$B = B_{\text{max}}L/(K_d + L)$$

where  $B$  is the concentration of bound ligand,  $B_{\text{max}}$  is the maximal number of binding sites,  $K_d$  is the ligand dissociation constant, and  $L$  is the ligand concentration.

*Competition Binding Studies:  $K_i$  Determination.* Competition binding was determined by incubating homogenates with a concentration of [ $^3\text{H}$ ]5 at approximately  $K_D$  in the presence of increasing concentrations of 17 or nonlabeled 5 ranging from 5 pM to 100 nM. The actual [ $^3\text{H}$ ]5 concentration added to the mixture was calculated by taking control counts of the experimental sample of [ $^3\text{H}$ ]5 to accurately calculate cpm/fmol per well. The concentration of cold compound that inhibited 50% of the specific binding of [ $^3\text{H}$ ]5 was determined ( $\text{IC}_{50}$ ). By use of the  $K_d$  and  $\text{IC}_{50}$  values obtained,  $K_i$  values were calculated according to Cheng and Prusoff:<sup>12</sup>  $K_i = (\text{IC}_{50}/(1 + (L/K_d)))$ .  $\text{IC}_{50}$  is the inhibitor concentration for half-maximal binding inhibition, and  $L$  is ligand concentration. The Y-axis in competition binding experiments is defined as the percent of control (POC).

*Ex Vivo Autoradiography.* Jugular cannulated SD rats were either dosed with [ $^3\text{H}$ ]5 (3, 10, 30, or 100  $\mu\text{Ci}$  iv) or pretreated with vehicle or 17 (10 mg/kg, po), and 50 min afterward, [ $^3\text{H}$ ]5 (30  $\mu\text{Ci}$ ) was administered by bolus intravenous injection via the jugular vein. Ten minutes after injection of the tracer, animals were euthanized by  $\text{CO}_2$  inhalation and brains were collected, frozen in ice-cold methylbutane (Sigma-Aldrich, St. Louis, MO), and stored at  $-80^{\circ}\text{C}$  until usage. Sagittal brain sections (20  $\mu\text{m}$ ) were cut on a cryostat (Leica, Nussloch, Germany) and air-dried, and autoradiographic images were acquired with a BetaIMAGER D (Biospace, Paris, France) and analyzed with M3vision (Biospace, Paris, France).

*Target Occupancy Analysis of 17.* A target occupancy dose–response study was conducted with 17. Sprague-Dawley (SD) rats were pretreated with vehicle (2% HPMC, 1% Tween 80, pH 2.2, with methanesulfonic acid) or 17 (0.1, 0.3, 1, 3, 10, and 30 mg/kg, po). Fifty minutes after dosing 17, 5 (6  $\mu\text{g}/\text{kg}$ ) was administered by bolus intravenous injection via lateral tail vein. Ten minutes after injection of 5, animals were euthanized and blood and brain samples (striatum as target tissue and thalamus as reference tissue) were collected. Brain samples were weighed and HPLC-grade water was added (20% weight/volume), followed by homogenization using a Covaris E210 acoustic homogenizer, as described previously. Homogenized samples were stored at  $-20^{\circ}\text{C}$  before analysis using API 4000 LC–MS/MS (Applied Biosystems, Carlsbad, CA).

PDE10A occupancy based on the reference tissue model was determined using the following equations:<sup>2,16</sup>

$$\text{BP} = (\text{STR} - \text{THA})/\text{THA} = (\text{STR}/\text{THA}) - 1$$

$$\text{RO}\% = 100 \times [1 - (\text{BP}_{\text{drug}}/\text{BP}_{\text{veh}})]$$

where BP refers to binding potential, RO refers to receptor occupancy,  $BP_{drug}$  refers to the binding potential of the test article dosed (17), and  $BP_{veh}$  refers to the binding potential of the vehicle.

Results were expressed as the mean  $\pm$  STD (standard deviation) or the mean  $\pm$  SEM (standard error of mean). Curve fit was assessed using a four-parameter nonlinear regression in GraphPad Prism software, version 5 (GraphPad Inc., San Diego, CA).

analysis:  $\log(\text{inhibitor})$  vs response – variable slope

equation:

$$Y = \text{bottom} + (\text{top} - \text{bottom}) / [1 + 10^{(\log EC_{50-x}) (\text{Hill slope})}]$$

Data outliers were determined using Grubb's test outlined in GraphPad Prism software (GraphPad Inc., San Diego, CA).

## AUTHOR INFORMATION

### Corresponding Author

\*For E.H.: phone (805) 313-5300; e-mail, ehu@amgen.com. For H.C.: phone, (650) 244-2490; e-mail, hangc@amgen.com.

### Present Address

<sup>∞</sup>Envoy Therapeutics, 555 Heritage Drive, Jupiter, Florida 33458, United States.

### Notes

The authors declare no competing financial interest.

## ACKNOWLEDGMENTS

We express our gratitude to Lee Phebus for his valuable insights and to David Bauer for his contributions to the experimental conditions.

## DEDICATION

We dedicate this paper to our dear friend and colleague Robert Cho who passed away in 2011. We will always be inspired by his dedication, talents, and kindness.

## ABBREVIATIONS USED

BP, binding potential; CMS, carboxymethyl 5; CNS, central nervous system; HCl, hydrogen chloride; HHBSS, Hepes buffered Hank's balanced salt solution; ID/g, injected dose per gram; LC–MS/MS, liquid chromatography coupled to mass spectrometry; PDE, phosphodiesterase; rbf, round-bottom flask; RO, receptor occupancy; SEM, standard error of the mean; SFC, supercritical fluid chromatography; SNAr, nucleophilic aromatic substitution; STR, striatum; THA, thalamus

## REFERENCES

(1) (a) Lee, C.; Parde, L. Using positron emission tomography to facilitate CNS drug development. *Trends Pharmacol. Sci.* **2006**, *27*, 310–317. (b) Wong, D. F.; Tauscher, J.; Grunder, G. The role of imaging in proof of concept for CNS drug discovery and development. *Neuropsychopharmacology* **2009**, *34*, 187–203. (c) Hargreaves, R. J. The role of molecular imaging in drug discovery and development. *Clin. Pharmacol. Ther.* **2008**, *83*, 349–353.

(2) (a) Soderling, S.; Bayuga, S.; Beavo, J. Isolation and characterization of a dual-substrate phosphodiesterase gene family: PDE10A. *Proc. Natl. Acad. Sci. U.S.A.* **1999**, *96*, 7071–7076. (b) Conti, M.; Beavo, J. Biochemistry and physiology of cyclic nucleotide phosphodiesterases: essential components in cyclic nucleotide signaling. *Annu. Rev. Biochem.* **2007**, *76*, 481–511. (c) Nishi, A.; Kuroiwa, M.; Miller, D. B.; O'Callaghan, J. P.; Bateup, H. S.; Shuto, T.; Sotogaku, N.; Fukuda, T.; Heintz, N.; Greengard, P.; Snyder, G. L. Distinct roles of PDE4 and PDE10A in the regulation of cAMP/PKA signaling in the striatum. *J. Neurosci.* **2008**, *28*, 10460–10471.

(3) (a) Seeger, T. F.; Bartlett, B.; Coskran, T. M.; Culp, J. S.; James, L. C.; Krull, D. L.; Lanfear, J.; Ryan, A. M.; Schmidt, C. J.; Strick, C. A.; Varghese, A. H.; Williams, R. D.; Wylie, P. G.; Menniti, F. S. Immunohistochemical localization of PDE10A in the rat brain. *Brain Res.* **2003**, *985*, 113–126. (b) Lakics, V.; Karran, E. H.; Boess, F. G. Quantitative comparison of phosphodiesterase mRNA distribution in human brain and peripheral tissues. *Neuropharmacology* **2010**, *59*, 367–374.

(4) (a) Siuciak, J. A.; McCarthy, S. A.; Chapin, D. S.; Fujiwara, R. A.; James, L. C.; Williams, R. D.; Stock, J. L.; McNeish, J. D.; Strick, C. A.; Menniti, F. S.; Schmidt, C. J. Genetic deletion of the striatum-enriched phosphodiesterase PDE10A: evidence for altered striatal function. *Neuropharmacology* **2006**, *51*, 374–385. (b) Siuciak, J.; McCarthy, S.; Chapin, D.; Martin, A.; Harms, J.; Schmidt, C. Behavioral characterization of mice deficient in the phosphodiesterase-10A (PDE10A) enzyme on a C57/Bl6N congenic background. *Neuropharmacology* **2007**, *54*, 417–427.

(5) (a) Verhoest, P. R.; Helal, C. J.; Hoover, D. J.; Humphrey, J. M. Heteroaromatic Quinoline Compounds. WO200607282 A2, 2006. (b) Kehler, J.; Ritzén, A.; Greve, D. The potential therapeutic use of phosphodiesterase 10 inhibitors. *Expert Opin. Ther. Pat.* **2007**, *17*, 147–158.

(6) (a) Grauer, S. M.; Pulito, V. L.; Navarra, R. L.; Kelly, M. P.; Kelley, C.; Graf, R.; Langen, B.; Logue, S.; Brennan, J.; Jiang, L.; Charych, E.; Egerland, U.; Liu, F.; Marquis, K. L.; Malamas, M.; Hage, T.; Comery, T. A.; Brandon, N. J. Phosphodiesterase 10A inhibitor activity in preclinical models of the positive, cognitive and negative symptoms of schizophrenia. *J. Pharmacol. Exp. Ther.* **2009**, *331*, 574–590. (b) Verhoest, P. R.; Chapin, D. S.; Corman, M.; Fonseca, K.; Harms, J. F.; Hou, X.; Marr, E. S.; Menniti, F. S.; Nelson, F.; O'Connor, R.; Pandit, J.; Proulx-LaFrance, C.; Schmidt, A. W.; Schmidt, C. J.; Siuciak, J. A.; Liras, S. Discovery of a novel class of phosphodiesterase 10A inhibitors and identification of clinical candidate 2-[4-(1-methyl-4-pyridin-4-yl-1H-pyrazole-3-yl)-phenoxy]methylquinoline (PF-2545920) for the treatment of schizophrenia. *J. Med. Chem.* **2009**, *52*, 5188–5196. (c) Farde, L.; Wiesel, F.; Halldin, C.; Sedval, G. Central D2-dopamine receptor occupancy in schizophrenic patients treated with antipsychotic drugs. *Arch. Gen. Psychiatry* **1988**, *45*, 71–76. (d) Sotty, F.; Montezinho, L.; Steiniger-Brach, B.; Nielson, J. Phosphodiesterase 10A inhibition modulates the sensitivity of the mesolimbic dopaminergic system to D-amphetamine: involvement of the D1-regulated feedback control of midbrain dopamine neurons. *J. Neurochem.* **2009**, *109*, 766–775. (e) Miyamoto, S.; Duncan, G. E.; Marx, C. E.; Lieberman, J. A. Treatments for schizophrenia: a critical review of pharmacology and mechanisms of action of antipsychotic drugs. *Mol. Psychiatry* **2005**, *10*, 79–104.

(7) (a) Simpson, E. H.; Kellendonk, C.; Kandel, E. A possible role for the striatum in the pathogenesis of the cognitive symptoms of schizophrenia. *Neuron* **2010**, *65*, 585–596. (b) Kehler, A. R.; Greve, D. R. The potential therapeutic use of phosphodiesterase 10 inhibitors. *Expert Opin. Ther. Pat.* **2007**, *17*, 147–158. (c) Hebb, A. L.; Robertson, H. A. Role of phosphodiesterases in neurological and psychiatric disease. *Curr. Opin. Pharmacol.* **2007**, *7*, 86–92. (d) Schmidt, C. J.; Chapin, D. S.; Cianfrogna, J.; Corman, M. L.; Hajos, M.; Harms, J. F.; Hoffman, W. E.; Lebel, L. A.; McCarthy, S. A.; Nelson, F. R.; Proulx-LaFrance, C.; Majchrzak, M. J.; Ramirez, A. D.; Schmidt, K.; Seymour, P. A.; Siuciak, J. A.; Tingley, F. D., III; Williams, R. D.; Verhoest, P. R.; Menniti, F. S. Preclinical characterization of selective phosphodiesterase 10A inhibitors: a new therapeutic approach to the treatment of schizophrenia. *J. Pharmacol. Exp. Ther.* **2008**, *325*, 681–690. (e) Menniti, F. S.; Faraci, W. S.; Schmidt, C. J. Phosphodiesterases in the CNS: targets for drug development. *Nat. Rev. Drug Discovery* **2006**, *5*, 661–670. (f) Halene, T. B.; Siegel, S. J. PDE Inhibitors in psychiatry—future options for dementia, depression and schizophrenia? *Drug Discovery Today* **2007**, *12*, 870–878. (g) Bender, A. T.; Beavo, J. A. Cyclic nucleotide phosphodiesterases: molecular regulation to clinical use. *Pharmacol. Rev.* **2006**, *58*, 488–520. (h) Kleiman, R. J.; Kimmel, L. H.; Bove, S. E.; Lanz, T. A.;

Harms, J. F.; Romegialli, A.; Miller, K. S.; Willis, A.; des Etages, S.; Kuhn, M.; Schmidt, C. J. Chronic suppression of phosphodiesterase 10A alters striatal expression of genes responsible for neurotransmitter synthesis, neurotransmission, and signaling pathways implicated in Huntington's disease. *J. Pharmacol. Exp. Ther.* **2011**, *336*, 64–76.

(i) Strick, C. A.; James, L. C.; Fox, C. B.; Seeger, T. F.; Menniti, F. S.; Schmidt, C. J. Alterations in gene regulations following inhibition of the striatum-enriched phosphodiesterase, PDE10A. *Neuropharmacology* **2010**, *58*, 444–451.

(8) (a) Barth, V.; Chernet, E.; Martin, L.; Need, A.; Rash, K.; Morin, M.; Phebus, L. A. Comparison of rat dopamine D2 receptor occupancy for a series of antipsychotic drugs measured using radiolabeled or nonlabeled raclopride. *Life Sci.* **2006**, *78*, 3007–3012. (b) Need, A. B.; McKinzie, J. H.; Mitch, C. H.; Statnick, M. A.; Phebus, L. A. In vivo rat brain opioid receptor binding of LY255582 assessed with a novel method using LC/MS/MS and the administration of three tracers simultaneously. *Life Sci.* **2007**, *81*, 1389–1396. (c) Chernet, E.; Martin, L. J.; Li, D.; Need, A. B.; Barth, V. N.; Rash, K. S.; Phebus, L. A. Use of LC/MS to assess brain tracer distribution in preclinical, in vivo receptor occupancy studies: dopamine D2, serotonin 2A and NK-1 receptors as examples. *Life Sci.* **2005**, *78*, 340–346. (d) Caldwell, R. L.; Caprioli, R. M. Tissue profiling by mass spectrometry. *Mol. Cell. Proteomics* **2005**, *394*–401.

(9) Arrington, M. P.; Liu, R.; Hopper, A. T.; Conticello, R. D.; Nguyen, T. M.; Gauss, C. M.; Burli, R.; Hitchcock, S. A.; Hu, E.; Kunz, R. Cinnoline Derivatives as Phosphodiesterase 10 Inhibitors, Their Preparation, Pharmaceutical Compositions, and Use in Therapy. WO 2007098169, 2007.

(10) (a) Passchier, J.; Gee, A.; Willemsen, A.; Vaalburg, W.; van Waarde, A. Measuring drug-related receptor occupancy with positron emission tomography. *Methods* **2002**, *27*, 278–286. (b) Wong, D. F.; Pomper, M. G. Predicting the success of a radiopharmaceutical for in vivo imaging of central nervous system neuroreceptor systems. *Mol. Imaging Biol.* **2003**, *5*, 350–362. (c) Schlyer, D. PET tracer and radiochemistry. *Ann. Acad. Med., Singapore* **2004**, *33*, 146–154.

(11) Multiple reactions monitoring (MRM) detection method using triple quadrupole mass spectrometry is currently the gold standard approach for quantitative analysis of drugs in complex matrices (e.g., plasma and brain tissue). In a typical MRM experiment, the precursor ion of the targeted analyte was first isolated in the first quadrupole (Q1), followed by fragmentation of the ions in the second quadrupole (Q2) using the collision induced dissociation method (CID). The last step of the MRM analysis is isolation of a characteristic product ion of the drug in the third quadrupole (Q3). The specificity and sensitivity of the method were primarily due to simultaneous detection of both precursor and product ions that are unique to the targeted drug candidate.

(12) Cheng, Y.; Prusoff, W. H. Relationship between the inhibition constant (K<sub>i</sub>) and the concentration of inhibitor which causes 50 percent inhibition (I<sub>50</sub>) of an enzymatic reaction. *Biochem. Pharmacol.* **1973**, *22*, 3099–3108.

(13) (a) Celen, S.; Koole, M.; De Angelis, M.; Sannen, I.; Chitneni, S. K.; Alcázar, J.; Dedeurwaerdere, S.; Moechars, D.; Schmidt, M.; Verbruggen, A.; Langlois, X.; Van Laere, K.; Andrés, J. I.; Bormans, G. Preclinical evaluation of <sup>18</sup>F-JNJ41510417 as a radioligand for PET imaging of phosphodiesterase-10A in the brain. *J. Nucl. Med.* **2010**, *51*, 1584–1591. (b) Andrés, J.-I.; De Angelis, M.; Alcázar, J.; Iturrino, L.; Langlois, X.; Dedeurwaerdere, S.; Lenaerts, I.; Vanhoof, G.; Celen, S.; Bormans, G. Synthesis, in vivo occupancy, and radiolabeling of potent phosphodiesterase subtype-10 inhibitors as candidates for positron emission tomography imaging. *J. Med. Chem.* **2011**, *54*, 5820–5853.

(14) Schinkel, A. H.; Wagenaar, E.; van Deemter, L.; Mol, C. A.; Borst, P. Absence of the mdr1a P-glycoprotein in mice affects tissue distribution and pharmacokinetics of dexamethasone, digoxin, and cyclosporin A. *J. Clin. Invest.* **1995**, *96*, 1698–1705.

(15) Karlsson, R.; Katsamba, P. S.; Nordin, H.; Pol, E.; Myszk, D. G. Analyzing a kinetic titration series using affinity biosensors. *Anal. Biochem.* **2006**, *349*, 136–147.

(16) Wadenberg, M.; Soliman, A.; VanderSpek, S. C.; Kapur, S. Dopamine D2 receptor occupancy is a common mechanism underlying animal models of antipsychotics and their clinical effects. *Neuropsychopharmacology* **2001**, *25*, 633–641.